

Nanostructured Electrodes – A Tool for Studying Mesoscopic Transport Effects in Electrocatalytic Reactions

R. Jürgen Behm¹, Yvonne E. Seidel¹, Rakel Wreland Lindström^{1,a}, Z. Jusys¹, U. Wiedwald², Paul Ziemann², Björn Wickman³, Bengt Kasemo³, Dan Zhang⁴, Olaf Deutschmann⁴

¹ Institut für Oberflächenchemie und Katalyse, Universität Ulm, D-89081 Ulm, Germany

² Institut für Festkörperphysik, Universität Ulm, D-89081 Ulm, Germany

³ Dept. of Applied Physics, Chalmers University of Technology, S-41296 Göteborg, Sweden

⁴ Institut für Technische Chemie und Polymerchemie, Universität Karlsruhe (TH), D-76131 Karlsruhe, Germany

Summary

The role of mesoscopic mass transport effects in electrocatalytic reactions was investigated experimentally, in flow cell measurements with controlled transport characteristics, and theoretically, using computational fluid dynamic (CFD) calculations coupled with reaction kinetics. Nanotechnology was used to produce nanostructured electrodes with well defined structural characteristics, which could be varied in a controlled way, as templates with ‘simple’ geometries for the CFD calculations. Electrodes with systematically structural characteristics were employed for model studies on reactions of increasing complexity, including CO oxidation (one product: CO₂), oxygen reduction reaction (ORR - two products: H₂O₂ and H₂O) and methanol oxidation (MOR - three possible products: HCOOH, HCHO and CO₂).

The electrodes consist of arrays of Pt ultra-microelectrodes of defined particle size and separation on planar glassy carbon supports, which were fabricated employing colloidal lithography techniques (group Prof. Kasemo) or by deposition of metal-salt loaded inverse micelles (group Prof. Ziemann). Electrocatalytic measurements reveal distinct variations not only in the rates, but also in the selectivities of the ORR and MOR, respectively, with the amounts of incompletely reacted products decreasing with increasing Pt nanodisc density and/or decreasing electrolyte flow. These observations are explained in a simple reaction model, involving desorption and repetitive re-adsorption and further reaction of desorbed incomplete reaction products on the Pt nanodiscs (‘desorption – re-adsorption – reaction’ mechanism) [1-3].

CFD calculations were carried out to explore the effect of mass transport processes on the overall reaction on the arrays of microelectrodes. Coupled with a detailed model of the reaction kinetics, the numerical simulations were used to determine profiles of the reactant concentration, coverage and velocity fields in time and space for a thin-layer flow cell. Simplified rate equations were derived based on a combination of physical and mathematical arguments. Monolayer CO_{ad} oxidation (CO_{ad} stripping) and continuous CO oxidation (CO bulk oxidation) are employed as probe reactions. The kinetic parameters were estimated by fitting the numerically predicted peak currents and peak potentials with experimental data. A non-linear variation of the activation energy with CO coverage is introduced, reflecting interaction energies between CO_{ad} species. Mass transfer limitations of the electrocatalytic reaction rate are found to primarily result from CO diffusion normal to the electrode. Satisfactory agreement between experiment and simulation on the planar and nanostructured Pt/GC model electrodes is achieved. Finally, future strategies in experiment and theory are discussed.

For publication in: *Functional Nanostructures II*, Springer Series *Nanoscience & Technology*, T. Schimmel and H. v. Löhneysen, Eds. (Springer-Verlag, Berlin – Heidelberg - New York – Tokyo, 2010).

^a pres. address: School of Chemical Science and Engineering, KTH (Royal Institute of Technology), SE-10044 Stockholm, Sweden

1 Introduction

In recent years, the interest in electrocatalytic reactions has rapidly increased because of their potential applications in Fuel Cell Technology [4-7]. In the present work, we want to explore a specific aspect of electrocatalytic reactions, which is highly relevant also for applications, but in most cases neglected in model studies, namely the influence of transport effects and transport processes on the electrocatalytic reaction process.

It is well known that in many electrocatalytic reactions the reaction rate is limited by the transport of reactants to the electrode, resulting in a "mass transport limited current" [8-12]. Less known is that transport effects may alter also the overall behavior of the reaction, in particular its selectivity and product distribution. This aspect is of interest in reactions where soluble or volatile reaction intermediates are formed. During reactions such as oxygen reduction or the oxidation of methanol, the resulting product distribution may change significantly for different transport conditions. Such effects have been reported previously, e.g., for the oxidation of methanol [13-15] or ethanol [16]. In the latter studies [15,16], these changes were explained by re-adsorption effects. Following this mechanism, a dissolved reaction intermediate can re-adsorb on the electrode and react further to a (stable) final product, with the re-adsorption probability depending on the transport conditions.

These trends can easily be followed and understood on a qualitative scale. So far, however, there was a lack of quantitative understanding, which is mostly due to the very complex transport situations in a thin-film catalyst electrode. Therefore, new experimental approaches were needed, where simple structures lead to better defined transport processes, which are more easily accessible to theoretical description by appropriate modelling and simulation procedures. Furthermore, modelling procedures have to be extended to allow a precise description of electrocatalytic reaction and transport effects on structurally well-defined electrodes under realistic conditions, in particular in a realistic flow cell with well-defined mass transport properties. This was topic of the present work, where we aimed at a quantitative description of electrocatalytic processes by combination of experimental studies using nanostructured Pt/glassy carbon (GC) electrodes with well defined structural properties and sophisticated modelling of the transport and reaction processes. The nanostructured electrodes are prepared by use of Colloidal Lithography techniques [17,18] or by deposition of inverse, metal-salt loaded micelles and a subsequent after-treatment [19]. The resulting electrodes consist of regularly arranged arrays of electrocatalytically active nanostructures/~particles on a planar, inert carbon substrate. Due to their known and well-defined surface morphology, these electrodes are ideally suited for the planned studies. These techniques allowed the variation of the density and the size or distribution of the nanostructures/~particle in a controlled way, which will directly affect the transport properties. In the same way, transport can be varied also by changing the electrolyte flow rate.

Based on studies using these nanostructured electrodes, we recently introduced the „desorption – re-adsorption – reaction“ model [1], which in addition to the direct formation of the reaction products includes indirect pathways, involving desorption of reactive intermediates,

which can subsequently either adsorb again or leave the diffusion layer and be transported away with the flowing electrolyte. Upon re-adsorption on electrocatalytically active material, the reaction intermediates may either react further or desorb again, which would start a new sequence (see schematic description in Fig. 1). Re-adsorption on inert substrate material, in contrast, would result in immediate desorption.

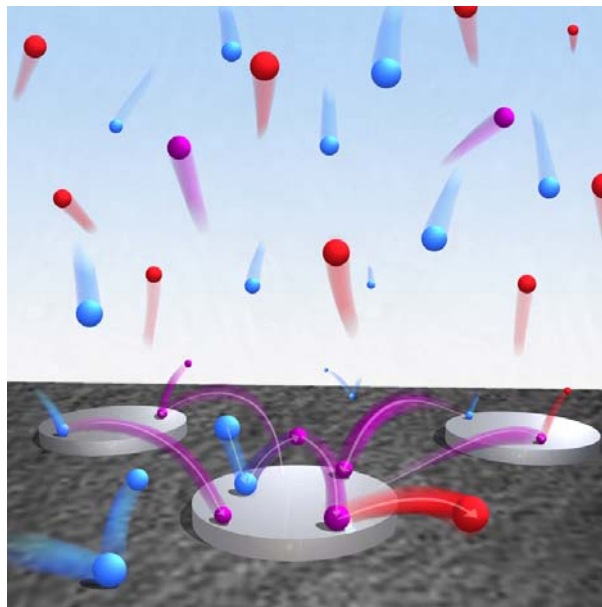


Fig. 1 Transport processes occurring during an electrocatalytic reaction on a nanostructured Pt/GC (glassy carbon) electrode: catalytically active Pt nanostructures of defined size (light grey) are deposited on an inert GC support (black). Incoming reactant molecules (blue) are adsorbed on a Pt nanostructure and react to a reaction intermediate (violet), which desorbs into the diffusion layer. This molecule can either re-adsorb on the same or on a neighboring Pt nanostructure, where it can further react to the final product (red), which then leaves the near electrode surface region, or the desorbed intermediate leaves the diffusion layer into the flowing electrolyte without further reaction (reproduced with permission from ref. [2]).

In the following section, we will present results of model studies on transport effects, where these effects were systematically explored by varying the density or size of the nanostructures or the electrolyte flow rate. In these studies, three different types of reactions were investigated; the mainly mass transport limited oxidation of CO (bulk oxidation), the mixed mass transport and kinetically limited oxygen reduction reaction, and the kinetically limited oxidation of formaldehyde and methanol. The results will be discussed in terms of the „desorption – re-adsorption – reaction“ model.

Parallel to the experimental studies, the electrocatalytic reactions were simulated numerically, combining mass transport and electrocatalytic kinetics. Since the measured reaction rate of the electrocatalytic reaction can be affected by concentration gradients in the cell, which can arise from the relatively slow diffusion in the liquid phase, the local concentrations of reactive species are important. Such variations would result in temporarily and spatially varying reaction conditions. Combining experimental data and simulations of reaction and transport allows a detailed interpretation of the measurements and has the potential for an in depth under-

standing, on a molecular scale, of the reaction process in the cell and the underlying reaction mechanism. In particular, it may help deriving information on the nature of the rate limiting step in more complex reaction networks.

In this contribution, the oxidation of a pre-adsorbed monolayer of CO (“CO_{ad} stripping”) and continuous CO oxidation (CO bulk) are employed as the probe reactions [20,21]. This is not only a standard reaction in electrocatalysis, but also plays an important role in the oxidation of small organic molecules such as methanol or ethanol oxidation reaction, which are of particular interest because of their potential application in fuel cell systems [22]. In these reactions, CO_{ad} is produced as side product or reaction intermediate, and acts as catalyst poison for Pt catalysts. The Faradaic current peak during oxidation of pre-adsorbed CO was investigated to obtain primary parameters of the kinetic model used, in particular the rate for CO oxidation, and the initial coverage of CO_{ad}. Based on these kinetic parameters, the influence of mass transport on electrocatalytic reactions was facilitated by comparing and reproducing the oxidation current profiles of continuous CO oxidation on polycrystalline Pt (pcPt) and medium density HCL-prepared Pt nanodiscs (disc diameter ~120 nm and covering about 20 %) on a planar glassy carbon (GC) support.

In principle, the velocity of a fluid around a nanostructured Pt/GC electrode should be described at a molecular scale. Obviously, this would be impractical owing to the large numbers of molecules that would have to be considered. It is more appropriate to use a velocity field that represents an average fluid velocity at every point within the fluid. Moreover, coverage dependent interaction energies between adsorbed CO_{ad} were introduced as an additional parameter [25,26].

In total, detailed insight into the mutual influence of transport processes and electrocatalytic reaction and the resulting overall process shall be gained by combining nanostructuring concepts from nanotechnology, electrochemical measurements under defined reaction and transport conditions, and sophisticated modelling of both transport and reaction processes.

2 Results and Discussion

2.1 Physical Characterization of the nanostructured Pt/GC electrodes by Scanning Electron Microscopy (SEM)

The morphology of the nanostructured electrodes was characterized by scanning electron microscopy (LEO 1550 - Zeiss, group of Prof. Fecht, Ulm University). SEM images of a continuous polycrystalline Pt film and of the GC supported nanostructured electrodes prepared via HCL or metal-salt loaded micelles are shown in Fig. 2. For a simplified description of the geometrical surface area of the resulting Pt nanostructures (after HCL procedure), they were modeled by vertical, flat Pt cylinders of 20 nm height. For the Pt nanoparticles resulting from the deposition of metal-salt loaded micelles, we assumed ideal spherical shape on the GC substrate surface. The structural characteristics of the Pt nanostructures and Pt nanoparticles are summarized in Table 1.

TABLE 1. SEM and electrochemical characterization of a polycrystalline Pt electrode and selected nanostructured Pt/GC electrodes prepared by Hole-Mask Colloidal lithography and metal-salt loaded micelles deposition, respectively. Geometric surface areas are calculated assuming a cylindrical shape for the nanodiscs and spherical shape for the nanoparticles.

Sample	Coverage / %	Particle Diameter / nm	Particle Density / μm^2	Geom. Surf. Area / cm^2	Act. Surf. Area / cm^2
pc Pt	100	--	--	0.283	0.501
HCL-20-60	17	55 ± 9	72	0.118	0.272
HCL-05-60	4	52 ± 8	17	0.029	0.045
HCL-20-100	22	118 ± 12	20	0.104	0.288
HCL-01-100	~ 1	95 ± 9	1.4	0.005	0.008
Pt micelles	$25^{*)}$	$25 \pm 5^{*)}$	610	$0.423^{*)}$	0.080
	$\sim 3^{**)}$	$8 \pm 2^{**)}$		$0.043^{**)}$	

^{*)} These values were obtained by SEM measurements. ^{**)} These values were obtained by AFM (particle heights) and TEM measurements. The deviation is ascribed to the formation of carbon ‘columns’ underneath the Pt particles due to overetching and/or carbon residues from the polymer.

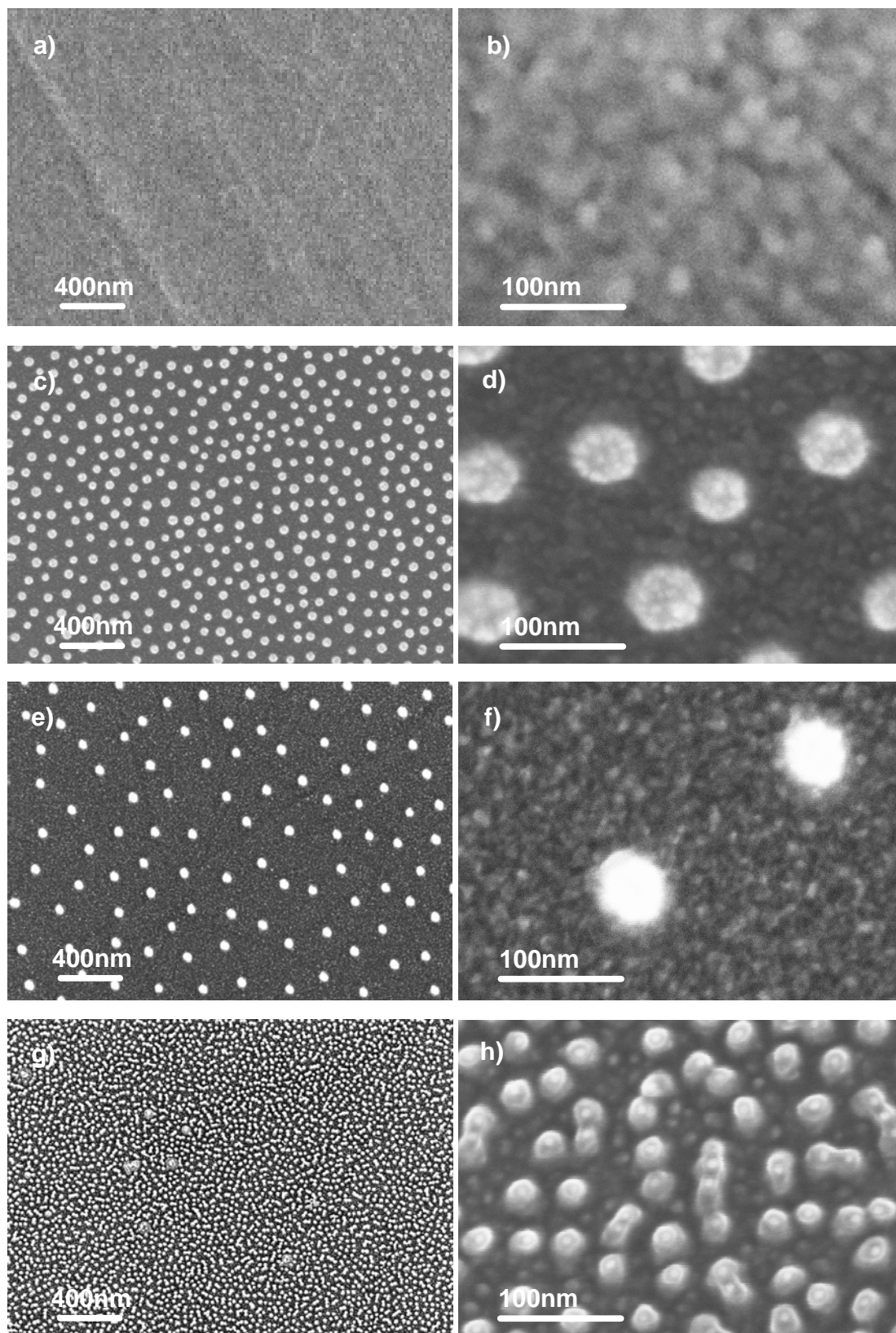


Fig. 2 Large-scale (Figs. 2a,c,e,g) and high-resolution (Figs. 2b,d,f,h) SEM images of a pristine Pt film (Figs. 2a,b), nanostructured Pt/GC electrodes fabricated by Hole-Mask Colloidal Lithography with high-density (Figs. 2c,d) and low-density Pt nanostructures (Figs. 2e,f) and a nanostructured Pt/GC electrode prepared by deposition of metal-salt loaded micelles (Figs. 2g,h). Large-scale images $2.9 \mu\text{m} \times 2.1 \mu\text{m}$; high-resolution images $360 \text{ nm} \times 260 \text{ nm}$.

2.2 Transport effects on the reaction rate: Continuous CO oxidation as a function of mass transport

As a first test reaction to illustrate the effect of mass transport on the nanostructured electrodes, we used a rather “simple” reaction with only one possible product, the oxidation of CO to CO₂. Under most conditions, the oxidation of CO to CO₂ is mainly mass transport limited and is therefore an excellent representative for studies upon mass transport effects. Fig. 3 shows the current traces for continuous CO bulk oxidation on a continuous Pt surface and on nanostructured Pt/GC electrodes. Overall, the different Pt/GC electrodes showed the reaction characteristics of polycrystalline Pt, independently of the preparation method. Interestingly, identical mass transport limited currents are obtained for a pc Pt electrode and nanostructured Pt/GC electrodes with Pt coverages down to a critical value (samples with ~20% of the surface covered by Pt nanostructures) [3]. Varying the electrolyte flow rate, a linear increase of the mass transport limited current I_{lim} with the cubic root of the electrolyte flow rate v was observed [27], in excellent agreement with the relation derived for a thin-layer flow cell [28]. The fact that the mass transport limited currents achieved at the same electrolyte flow rate (Fig. 3a) do not decay in the same way as the Pt coverage (as given in Table 1) indicates an increasing current density per Pt surface area with decreasing density of the Pt nanostructures (Fig. 3b). This fits perfectly to the increasing current density at the transition from planar diffusion to hemispherical diffusion [29]. Similar trends were recently reported by Morf [30], who calculated the transport limited current over arrays of ultra-microelectrodes on a planar, inert substrate in a flow cell under continuous electrolyte flow conditions in a simplified way, by assuming a constant reactant concentration at the upper boundary of a boundary layer of a given thickness [31]. The simulations demonstrated a constant mass transport limited current with decreasing particle density or coverage, respectively, until a critical value of the density of ultra-microelectrodes was reached. Above this value, the diffusion spheres over the individual microelectrodes overlap and result in a planar diffusion geometry at larger distances to the electrode surface, which is comparable to that above a non-structured reactive electrode surface (see Fig. 4a). Below that critical density/coverage of the ultra-microelectrodes, the overlap between the diffusion spheres decreases, and the diffusion limited current approaches that of a sum of independent microelectrodes on the electrode-surface [30].

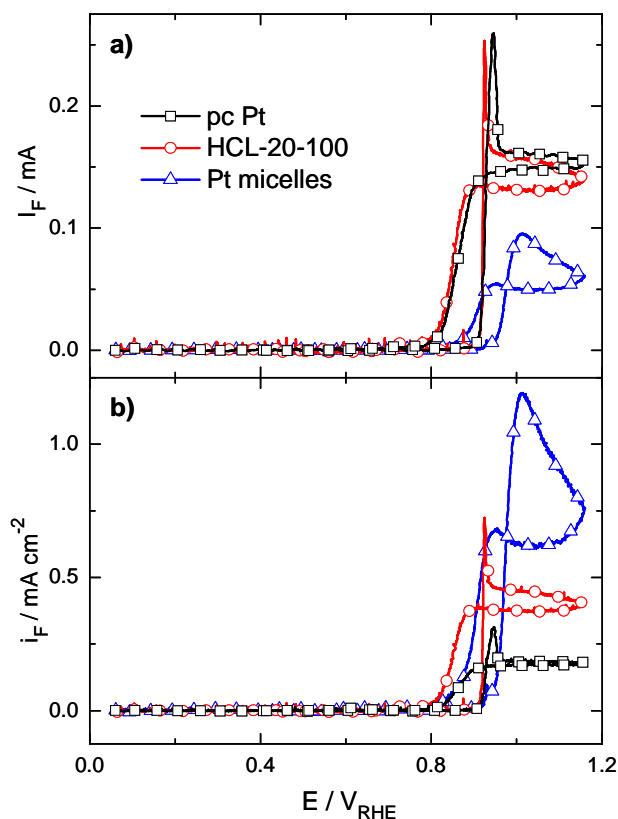


Fig. 3 Continuous potentiodynamic CO bulk electrooxidation on different electrodes in CO-saturated 0.5 M H_2SO_4 solution at room temperature. Faradaic currents (a) and current densities normalized vs. their respective active surface area as given in Table 1 (b) for a pc Pt electrode (squares), a medium-density nanostructured Pt/GC electrode prepared by HCL (HCL-20-100) (circles) and a nanostructured Pt/GC electrode prepared by deposition of Pt-salt loaded micelles (triangles).

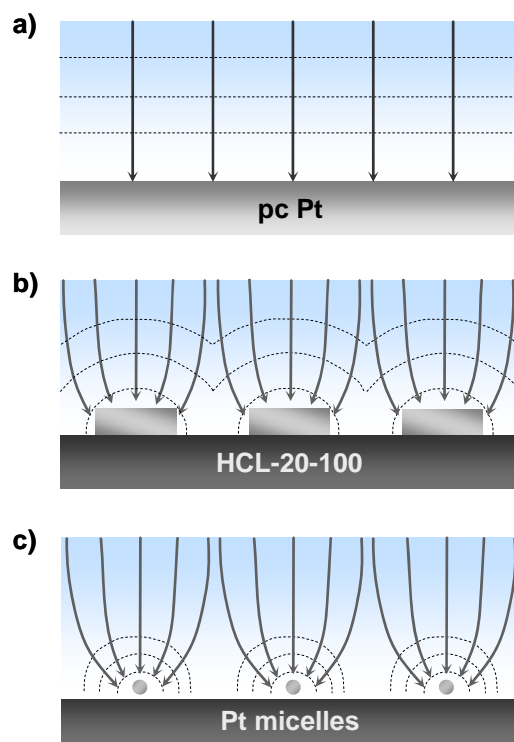


Fig. 4 Schematic description of the diffusion field during a mass transport limited reaction (CO bulk oxidation) over (a) a planar pc Pt electrode ('planar diffusion'), (b) a nanostructured Pt/GC electrode with high Pt coverage, e.g. HCL-20-100, with contributions from 'hemispherical diffusion' close to the nanostructures and transformation to almost 'planar diffusion' further away from the electrode, and (c) a nanostructured Pt/GC electrode prepared by deposition of metal-salt loaded micelles, e.g., Pt-micelles ('hemispherical diffusion'). Dashed lines: lines of constant CO concentration.

2.3 Transport effects on the selectivity: O_2 reduction and HCHO oxidation

In the next step, more complex reactions such as the reduction of oxygen to water (which is the reaction at the cathode of a low temperature PEM fuel cell) and the oxidation of formaldehyde to CO_2 were investigated. Both reactions have in common, that two possible products may be formed, depending on the respective reaction conditions. The possible undesired by-products of the given reactions are H_2O_2 during the oxygen reduction and formic acid which during formaldehyde oxidation. In this section, we will discuss the influence of the Pt coverage on the selectivity (resulting product distribution) in the two reactions, in the oxygen reduction reaction (ORR) and in the formaldehyde oxidation reaction (FOR).

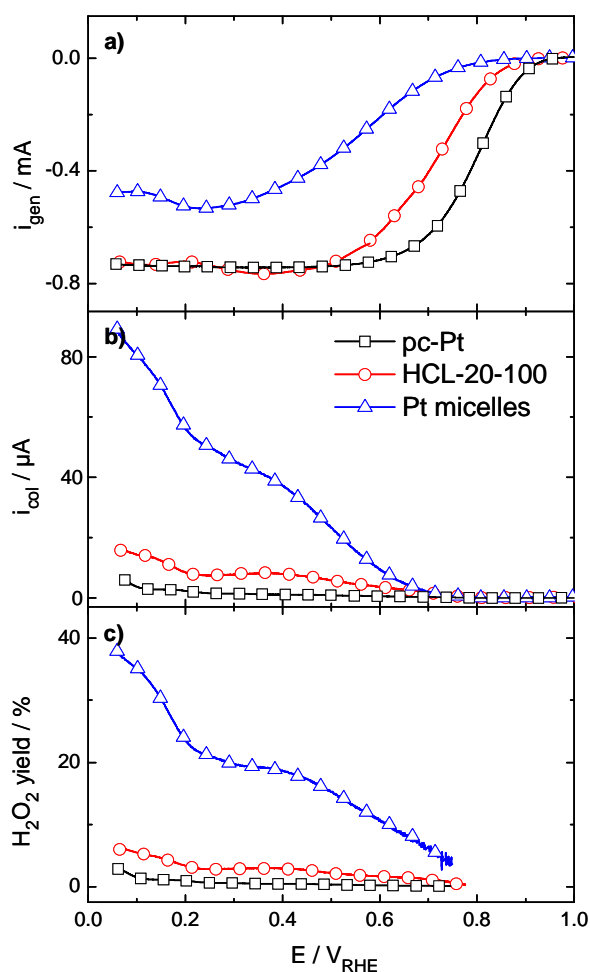


Fig. 5 Oxygen reduction activity (a), hydrogen peroxide oxidation at a smooth polycrystalline Pt collector electrode biased at 1.2 V (b), and the corresponding hydrogen peroxide yields (c) on a pc Pt sample (squares) and nanostructured Pt/GC electrodes prepared by HCL (HCL-20-100) (circles) by deposition of Pt-salt loaded micelles (triangles).

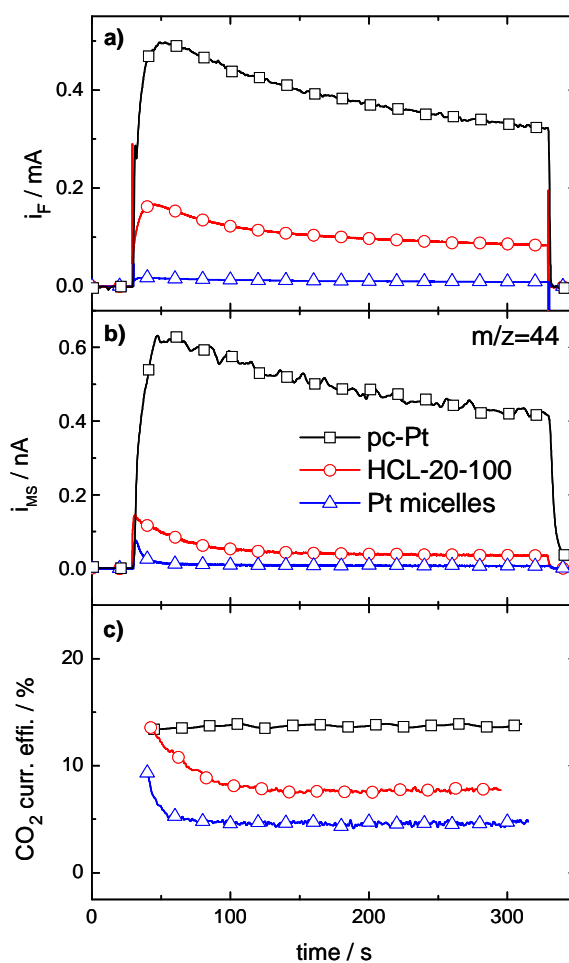


Fig. 6 Continuous (bulk) potentiostatic HCHO electrooxidation on pc Pt sample (squares) and nanostructured Pt/GC electrodes prepared by HCL (HCL-20-100) (circles) and a nanostructured Pt/GC electrode prepared by deposition of metal-salt loaded micelles (triangles) in 0.5 M H_2SO_4 + 0.1 M HCHO at room temperature. Faradaic currents (a), mass spectrometric currents at $m/z=44$ (b) and CO_2 current efficiencies (c). The potential was stepped from 0.06 V to 0.76 V at a constant flow rate of $10 \mu L s^{-1}$.

Starting with the ORR, the overall reaction current obtained on the different electrodes is shown in Fig. 5a. In general, the Faradaic currents reflect the well-known characteristics of pc Pt electrodes [32], which are represented by the squares in Fig. 5a. These include a well-resolved mass transport limited region (potentials from 0.06 to ca. 0.5 V), followed by a mixed mass transport/kinetically limited region (potentials positive of 0.5 V up to ~ 0.9 V), and finally a purely kinetically limited region at potentials positive of 0.9 V. Also in this case, the mass transport limited current decays only after the Pt coverage falls short of a critical value. It is not affected when changing from pc Pt to the HCL-20-100 sample, but decreases

significantly when going to the Pt micelles sample. The explanation is the same as that given before for CO bulk oxidation (section 2.2 and ref. [3].) Here, the main focus lies on the ORR selectivity (product distribution), which is reflected by the fractional yields of H₂O and H₂O₂ (Fig. 5c). On pc Pt and on the nanostructured Pt/GC electrode with high Pt coverage prepared by HCL, only small amounts of H₂O₂ are formed at E < 0.3 V, whereas on the sample with low Pt coverage (Pt micelle sample) the H₂O₂ yield is significantly higher, at least 10-fold higher in comparison to pc Pt, and H₂O₂ formation starts already at a potential of ~0.8 V. - Obviously, the H₂O₂ yield increases with increasing separation of the Pt nanostructures. This observation agrees perfectly with expectations based on the „desorption – re-adsorption – reaction“ model, which will be discussed in detail below.

Representative Faradaic and mass spectrometric transients for potentiostatic formaldehyde oxidation are shown in Fig. 6. It is important to note that under the given reaction conditions the FOR is not mass transport limited, but kinetically controlled. The current transients are characterized by a rapid initial increase of I_F upon stepping the potential from 0.06 to 0.76 V, leading to a maximum after about 20 s. The further development is dominated by a continuous decrease of the current (Fig. 6a). Qualitatively similar characteristics are obtained also for the MS signals (m/z=44, Fig. 6b). The absolute values of the Faradaic current and of the CO₂ formation rate decrease with increasing separation of the Pt nanostructures (see also above). The current efficiency for CO₂ formation (Fig. 6c) has its highest value in the initial phase, right after the potential step, and then the CO₂ current efficiency decreases to reach an approximately constant value after about 100 s. The steady-state CO₂ current efficiency measured after 5 minutes is around 13% for the pc Pt sample, but only 8% for the HCL-type sample (HCL-20-100), and below 5% micelle based nanostructured Pt/GC electrode. Correspondingly, the probability for formic acid formation increases measurably with decreasing density of Pt nanostructures/-particles.

Obviously, the reaction selectivity for ORR and FOR was affected by changing the Pt coverage. The measurements demonstrate that with increasing separation between the Pt nanostructures (= lower Pt coverage), the amount of incompletely reacted reaction intermediates such as H₂O₂ or formic acid also increases. This observation fully agrees with predictions from the “desorption – re-adsorption – reaction” model described in the introduction and in ref. [33]. In that model, the lower Pt coverage leads to a decreasing probability for re-adsorption and hence also for further oxidation of re-adsorbed incomplete reaction products H₂O₂ or formic acid on the active Pt nanostructures. Correspondingly, the off-transport of dissolved H₂O₂ or formic acid molecules, respectively, and hence the measured product yield of these species increases. These findings are consistent with concepts developed in Heterogeneous Catalysis, where it is well known that with decreasing space velocity (higher catalyst loading at constant reactant flow, or lower reactant flow at constant catalyst loading) the system and therefore also the product distribution moves towards the thermodynamic equilibrium product composition [34].

Correspondingly, similar effects can also be expected for varying the electrolyte flow. This will be discussed in the next section.

2.4 Transport effects on the selectivity due to variations in the electrolyte flow rate: Methanol oxidation

As a second important parameter for transport effects we investigated the influence of the electrolyte flow rate on the reaction characteristics. For reactions producing incomplete reaction intermediates such as the methanol oxidation reaction (MOR), variations of the electrolyte flow rate will not only affect the diffusion of reactants to the electrode, due to the variation in the thickness of the diffusion layer, but also modify the back diffusion of reaction intermediates (and products) through the diffusion layer into the flowing electrolyte. Therefore, also the probability for re-adsorption of desorbed reaction intermediates is affected.

The MOR represents a rather complex electrocatalytic reaction network, involving several reaction steps and intermediates such as formaldehyde and formic acid, in addition to the stable final product CO_2 [35]. To specifically address mass transport effects, we varied the electrolyte flow rate over a wide range, from $30 \mu\text{L s}^{-1}$ to very low values ($1 \mu\text{L s}^{-1}$). The resulting Faradaic currents and the CO_2 signals were converted into CO_2 current efficiencies. The values obtained after 180 s of continuous methanol oxidation on pc Pt, a HCL-20-60 and a HCL-05-60 sample are plotted in Fig. 7 vs. the electrolyte flow rate.

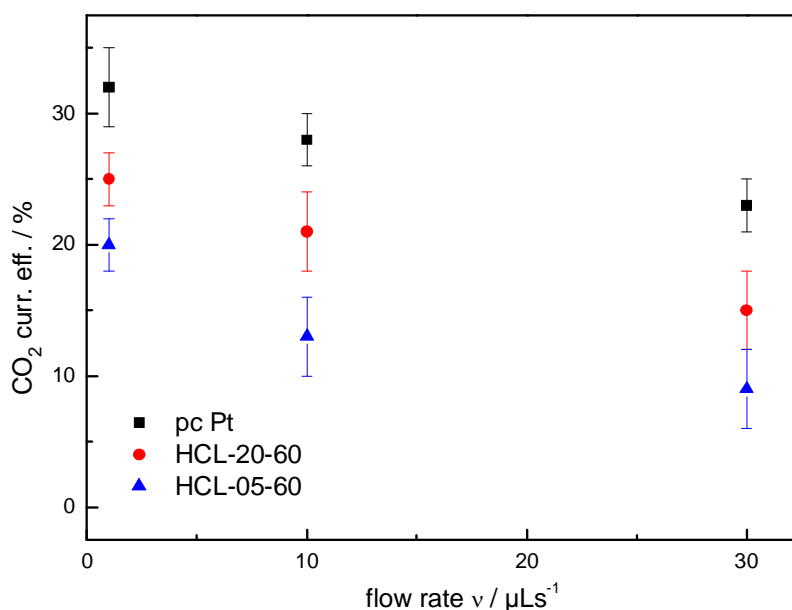


Fig. 7 Plot of the CO_2 current efficiencies after 180 s of continuous potentiostatic electrooxidation of methanol at 0.76 V on pc Pt (squares) and nanostructured Pt/GC electrodes with high (circles) and low (triangles) Pt coverage vs. the electrolyte flow rate v .

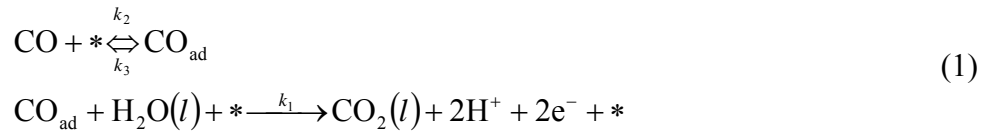
Obviously, the CO_2 current efficiency depends significantly (i) on the Pt coverage (vertical trend) and, though less, (ii) also on the electrolyte flow rate (from left to right side) and hence on the thickness of the diffusion layer. These trends agree fully with previous results obtained on massive electrodes or on electrodes covered by a thin-film of catalyst [13], and agree fully with the predictions derived from the “desorption – re-adsorption – reaction” model [14,15,33]. With increasing flow rate the thickness of the diffusion layer decreases, and there-

fore the lifetime of desorbed reaction intermediates in the diffusion layer decreases as well. Hence, the probability for re-adsorption of the reaction intermediates HCHO and HCOOH decreases with increasing electrolyte flow, and the CO₂ yield decreases, as observed experimentally. Finally, it should be noted that the effect of the flow rate is particularly pronounced on the higher Pt coverage samples (pc Pt and HCL-20-60), with their higher probabilities for re-adsorption at active Pt sites.

2.5 Modeling of CO oxidation mechanism

In this part, we present results of our efforts to develop a multi-scale approach for simulating electrocatalytic reactions on the nanostructured electrodes, where the simulations include both the actual electrocatalytic reaction and the transport of reactants and products. Following the experimental work, we will start with the electrooxidation of CO.

The analysis of the reaction mechanism begins with the assumption that the oxidation of CO_{ad} proceeds via the following scheme, in which one overall reaction can be deduced with the fact that all electron transfer comes from H₂O as follows



2.6 Effects of the different transport models on the Faradaic current

In a zero-dimensional model (0D), where no concentration gradients appear in the cell, only the reaction kinetics matters. Here, the CO_{ad} coverage approaches zero, consequently, CO desorption can be ignored. If the Faradaic current is controlled by the reaction kinetics, the adsorption rate constant k_2 can be described by the current I_F^{ss} , a quasi steady-state Faradaic current in the CO continuous oxidation, according to the following equations:

$$\begin{cases} \theta_{\text{CO}} \cong 0 \\ I_F^{ss} = F \int_s 2k_1 \theta_{\text{CO}} \rho_A [(1 - \theta_{\text{CO}}) \rho_A]^\beta ds \\ -k_1 \theta_{\text{CO}} [(1 - \theta_{\text{CO}}) \rho_A]^\beta + k_2 c_{\text{CO}} (1 - \theta_{\text{CO}}) - k_3 \theta_{\text{CO}} \cong 0 \end{cases} \Rightarrow I_F^{ss} \cong 2FA_{\text{cat}} k_2 c_{\text{CO}} \quad (2)$$

It is expected that all kinetic parameters need to be adjusted when different transport models are used; the set derived from the 0D model will serve as starting point for the more complex models.

Going to a one-dimensional (1D) model, where only flow parallel to the electrode is considered, no adequate set of kinetic parameters were found to produce acceptable agreement between computed and experimentally measured I_F curves using the mean velocity estimated from the residence time. The experimental I_F curve could only be reproduced by decreasing the inlet velocity dramatically. In other words, the 1D model failed; the resulting

rather small mean velocity $v_{m, fit} = 1.86 \times 10^{-3} \text{ m/s}$ indicates that other mass transport processes control the process of CO adsorption.

Next, we carried out simulations with a two-dimensional (2D) model, where also mass transport normal to the electrode is considered. Since mass transport normal to the electrode is dominated by diffusion, the CO profile in the fluid clearly reveals the strong effect of CO diffusion on the CO bulk oxidation. It means the overall electro-catalytic reaction rate is partly mass transport limited.

A full transient 3D simulation is applied to study mass transport in the cross section of the flow cell and to reveal other three-dimensional transport effects, which are caused by the three-dimensional structure of the cell with one inlet in the centre and four outlets at the cell periphery and not considered so far due to the simplifying assumptions made in the 1D and 2D models could have been overlooked so far. The kinetic parameters used in the 3D models are the ones derived in the 2D model. Figure 8 illustrates the predicted velocity distribution in the entire flow cell. Slices of the velocity distribution in Fig. 8a reveal a drastic increase of the velocity close to both the inlet and outlets of the cell; the maximum velocity ($5.46 \times 10^{-2} \text{ m/s}$) is about 10 times higher than the average inlet velocity. Fig. 8b illustrates that in the zones between two neighboring outlets the velocity is very low. This may lead to local mass transport limitations due to low convection in those zones. Although in reality three-dimensional CO concentration patterns are formed in the cell during the electrocatalytic CO oxidation on the electrode, the 3D and the 2D model lead to almost identical predictions of the

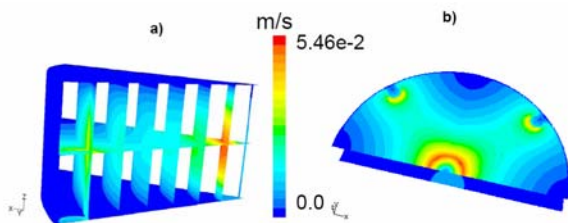


Fig. 8 Prediction of the 3D velocity distribution: (a) slices of the velocity field and (b) velocity distribution in the cross section.

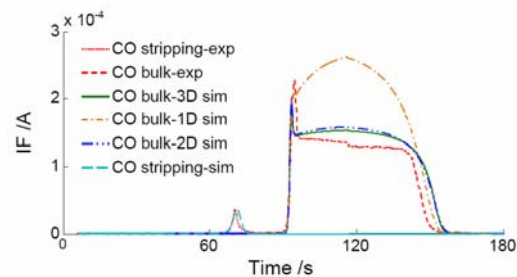


Fig. 9 Predicted and experimental profiles of the Faradaic current versus sweep time in CO_{ad} stripping and CO bulk oxidation (1D, 2D and 3D models).

Faradaic current profiles as shown in Fig. 9. Therefore, we conclude that CO diffusion in the direction normal to the electrode has a much more pronounced effect on the Faradaic current than lateral diffusion.

2.7 Optimization of kinetic data Δf

In the initial calculations, we assumed a constant interaction energy Δf at a given sweep rate. This value may be understood in the following way. A positive value of Δf indicates repulsive interaction and a negative value indicates an attractive interaction. When the CO_{ad} cover-

age is high, repulsive interactions between adsorbed CO molecules dominate. In contrast, when the CO_{ad} coverage is low, attractive interactions may affect the reaction. As a result, the value of Δf will depend on CO_{ad} coverage. In other words, the interaction energy changes with the coverage. The relation between the CO_{ad} coverage and the interaction energy Δf was fitted at different sweep rates as shown in Fig.10 to reproduce all Faradaic current waves. It is readily apparent that the value of Δf becomes smaller at coverages close to saturation (unity) and much larger at small coverage. In the intermediate region, it appears to be almost constant. The values of Δf at different sweep rates are a bit different. Fig. 10 also shows that the intermediate region of constant Δf decreases at low sweep rate and increases at high sweep rate. The tailing peak part of Δf is delayed with increasing sweep rates. However, an average value still could be taken to reflect the intrinsic nature of Δf .

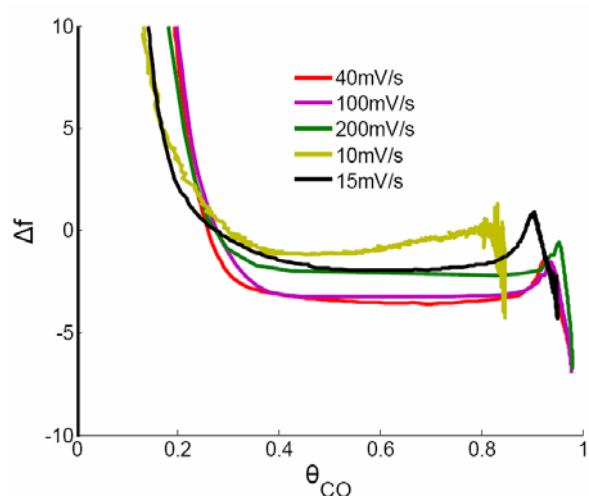


Fig. 10 Estimation of the interaction energy Δf on pc Pt.

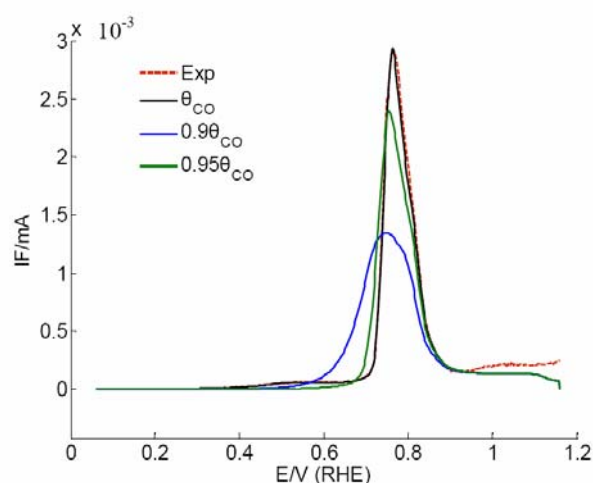


Fig. 11 Effects of the initial CO_{ad} coverage on the stripping voltammetry.

2.8 Formation of current peaks on nanostructured Pt/GC electrode

In this section, we systematically study the effect of the kinetic parameters of the CO_{ad} oxidation rate on the Faradaic current. The electric charge could be calculated by time-integration of the Faradaic current. In case of CO_{ad} stripping, the electric charge is given by the amount of CO_{ad} at saturation. In turn, the density of active sites can be deduced from the amount of CO_{ad} . The density of active sites on the pc Pt electrode is less than that on the medium density HCL-prepared nanostructured Pt/GC electrode, as shown experimentally by its much lower active surface area.

The oxidation rate k_1 strongly affects the full width half maximum (FWHM) and the peak potential of the Faradaic current. Figure 12 shows the Faradaic current calculated at different initial CO_{ad} coverages $\theta_{\text{CO}}^0 = 0.89$ and $\theta_{\text{CO}}^0 = 0.99$. We find a negative shift of approximately 60 mV when θ_{CO}^0 is increased by about 0.1 as shown in Fig. 11. This effect resembles the so-

called pre-wave in CO_{ad} oxidation which was reported by numerous authors and which is generally attributed to repulsive interactions between CO_{ad} at high coverages [6,36]. In our present mechanism, this repulsive interaction is considered by Δf . The value of Δf becomes large at coverage close to unity, which results in an increase of oxidation rate. Consequently, the peak current will appear at lower potential.

Another factor influencing the peak current is the CO_{ad} desorption rate. Although this rate is very low, it can create more vacant active sites to supply CO molecules adsorbed in the proceeding of CO bulk oxidation. Simulation shows that it plays a significant role in initiation of CO bulk oxidation.

Figure 12 shows a comparison of the experimental and simulated current for various inlet velocities. All kinetic parameters are derived by fitting the simulations with experiments. The simulation results show that the quasi steady-state Faradaic currents will be close along with the increase of inlet velocity. Figure 13 illustrates the concentration gradient of CO in the cell at different flow rates, which result from the diffusion of CO molecule in vertical direction.

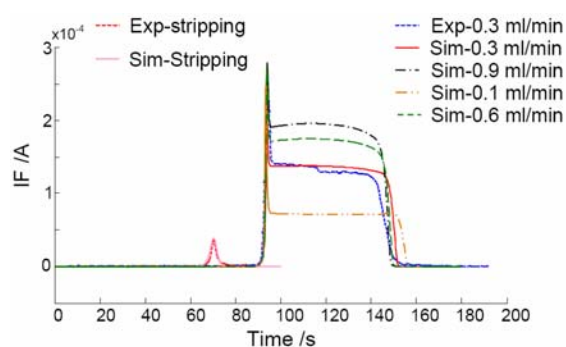


Fig. 12 Predictions of bulk voltammetry profiles at different inlet velocities..

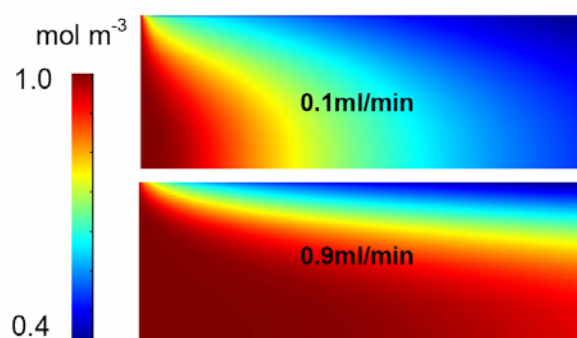


Fig. 13 Predicted distribution of the CO concentration in the cell during CO bulk oxidation.

3 Conclusions

The role of mesoscopic transport effects in electrocatalytic reactions was investigated experimentally and theoretically under controlled electrolyte transport conditions, using nanostructured Pt/GC electrodes with a well defined and rather simple morphology as model system. The nanostructured electrodes consist of arrays of electrochemically active Pt nanostructures of variable size, separation and distribution on an inert planar GC substrate. They are prepared via Hole-Mask Colloidal Lithography or by deposition of inverse metal-salt loaded micelles and a subsequent after-treatment. The experimental studies included different types of electrocatalytic reactions, ranging from mainly mass transport limited oxidation of CO, via the mixed mass transport limited and kinetically limited reduction of oxygen to the kinetically

limited oxidation of formaldehyde and methanol. Simulations concentrated on the oxidation of CO.

We could show that with increasing separation of the Pt nanostructures/~particles, the mass transport limited current for CO oxidation decreases less than expected from the decrease in Pt coverage. This is explained by a transition from 'planar diffusion' to 'hemispherical diffusion' of CO molecules to the active Pt surface, which leads to an increasing current density with decreasing Pt coverage.

Changes in the selectivity in the oxygen reduction reaction, in the formaldehyde oxidation reaction and in the methanol oxidation reaction upon varying the Pt nanostructure coverage or the electrolyte flow rate, with increasing yields of the stable final reaction product H₂O or CO₂, respectively, are explained in terms of the "desorption – re-adsorption – reaction" model. According to that model, an increasing probability of re-adsorption and further reaction of reaction intermediates such as H₂O₂, formaldehyde or formic acid leads to higher yields of the final products. The probability for re-adsorption increases with decreasing space velocity, i.e., with increasing Pt coverage or decreasing electrolyte flow.

In future, we plan expand the experimental work towards smaller particles, at and below the size of realistic catalyst particles (3 nm) down to clusters of few atoms only. Furthermore, in close interaction with theoretical simulations, the effects of the "desorption – re-adsorption – reaction" processes on the selectivity in electrocatalytic reactions involving desorbable intermediates shall be explored in more detail, aiming of a quantitative description of the re-adsorption processes. In the end, this would allow to derive probabilities for reaction during a single adsorption event ('single hit probabilities'). This way, transport effects could be fully separated from the description of the electrocatalytic reaction, and experimental data could be directly compared with results of ab-initio calculations such as density functional calculations, (DFT) which at present is not possible due to the contributions from transport effects in the experimental data.

In the simulations, a detailed electrocatalytic reaction mechanism, including the influence of the CO_{ad} coverage on the rates for adsorption, desorption, and oxidation of CO was coupled with transport models to numerically simulate the behavior of a dual thin-layer flow cell with pc Pt and a HCL-prepared nanostructured Pt/GC electrode. Two experimental procedures were analyzed; the oxidation of a preadsorbed CO monolayer (CO_{ad} stripping) and CO bulk oxidation at continuous flow of a CO saturated electrolyte.

In the model, the kinetic parameters were adapted step-by-step from the 0D to a 3D transport model. The CO desorption rate constant, k_3 , was shown to sensitively affect the full width at half maximum of the Faradaic current peak, while the onset of the current peak was affected by the oxidation rate constant, k_1 . For CO bulk oxidation, the onset of the current peak was affected by the reaction order β , and the number of free pc-Pt sites. The coverage dependent CO adsorption rate k_2 determines the quasi steady-state Faradic current.

The 2D and 3D models quantitatively reproduce all features of the potential dependent Faradaic current. It is shown that the cell does not represent a homogeneous system and that spatial and temporal gradients in the cell need to be taken into account for a thorough interpretation of the experimental data. CO concentrations and coverage depend on the positions in the cell and on the electrode, respectively. A non-linear dependence of the CO_{ad} oxidation rate on the CO_{ad} coverage is proposed, which reflects the changes in interaction energy with CO_{ad} coverage on the electrode surface.

The models and computer codes developed can not only be used to interpret the experimental findings, but also allow us to further explore the influence of the operating conditions. In future, the reaction kinetics shall be derived from the molecular behavior on the electrode rather than from a fit to measured data [37,38]. Current work is devoted to both of these directions

Acknowledgements

This work was supported by the Landesstiftung Baden-Württemberg via the Kompetenznetz Funktionelle Nanostrukturen (project B9), by the Ministry of Science, Research and the Arts of Baden-Württemberg and the European Social Fund (ESF) within the Schlieben-Lange-Programm, MISTRA (Contract No. 95014) and the Swedish Energy Agency (Grant No. P12554-1). We gratefully acknowledge A. Minkow (Institute of Micro- and Nanomaterials, Ulm University) for the SEM images.

References

1. A. Schneider, L. Colmenares, Y.E. Seidel, Z. Jusys, B. Wickman, B. Kasemo, and R.J. Behm, *Transport effects in the oxygen reduction reaction on nanostructured, planar glassy carbon supported Pt/GC model electrodes*, Phys. Chem. Chem. Phys. **10** (2008) 1931-1943.
2. Y.E. Seidel, A. Schneider, Z. Jusys, B. Wickman, B. Kasemo, and R.J. Behm, *Mesoscopic mass transport effects in electrocatalytic processes*, Faraday Discuss. **140** (2008) 167-184.
3. R. Lindström, Y.E. Seidel, Z. Jusys, M. Gustavsson, B. Kasemo, and R.J. Behm, *Electrocatalysis and transport effects on nanostructured Pt/GC electrodes*, J. Electroanal. Chem. (2009), doi:10.1016/j.jelechem.2009.04.034.
4. T. Iwasita-Vielstich, in *Advances in Electrochemical Science and Engineering*, H. Gerischer and C. W. Tobias, Eds. (VCH Verlagsgesellschaft, Weinheim, 1990).
5. W. Vielstich and T. Iwasita, in *Handbook of Heterogeneous Catalysis*, G. Ertl, H. Knözinger, and J. Weitkamp, Eds. (Wiley-VCH, Weinheim, 1997), Vol. 4.
6. N.M. Markovic and P.N. Ross Jr., Surf. Sci. Rept. **45** (2002) 117-229.
7. R.J. Behm and Z. Jusys, *The potential of model studies for the understanding of catalyst poisoning and temperature effects in polymer electrolyte fuel cell reactions*, J. Power Sources **154** (2006) 327-342.

8. H. Gerischer, I. Mattes, and R. Braun, *J. Electroanal. Chem.* **10** (1965) 553-567.
9. V.G. Levich, *Physicochemical Hydrodynamics* (Prentice Hall, Eaglewood Cliffs, NJ, 1962).
10. W.J. Albery, C.C. Jones, and A.R. Mount, in *Chemical Kinetics*, R.G. Compton and A. Hamnett, Eds. (Elsevier Publ., Amsterdam-Oxford-New York-Tokyo, 1986), Vol. 29.
11. C.M.A. Brett and A.M.F.C. Oliveira Brett, in *Chemical Kinetics*, C.H. Bamford and R.G. Compton, Eds. (Elsevier Publ., Amsterdam-Oxford-New York-Tokyo, 1986), Vol. 26.
12. J.A. Cooper and R.G. Compton, *Electroanal.* **10** (1998) 141-155.
13. H. Wang, Ch. Wingender, H. Baltruschat, M. Lopez, and M.T. Reetz, *J. Electroanal. Chem.* **509** (2001) 163-169.
14. H. Wang, T. Löffler, and H. Baltruschat, *J. Appl. Electrochem.* **31** (2001) 759-765.
15. Z. Jusys, J. Kaiser, and R.J. Behm, *Methanol electrooxidation over Pt/C fuel cell catalysts - Dependence of product yields on catalyst loading*, *Langmuir* **19** (2003) 6759-6769.
16. H. Wang, Z. Jusys, and R.J. Behm, *Ethanol electrooxidation on a carbon-supported Pt catalyst: Reaction kinetics and product yields* *J. Phys. Chem. B* **108** (2004) 19413-19424.
17. F. Burmeister, C. Schäfle, B. Keilhofer, C. Bechinger, J. Boneberg, and P. Leiderer, *From Mesoscopic to nanoscopic Surface Structures: Lithography with Colloid Monolayers*, *Adv. Mater.* **10** (1998) 495-497.
18. H. Fredriksson, Y. Alaverdyan, A. Dmitiev, C. Langhammer, D.S. Sutherland, M. Zäch, and B. Kasemo, *Adv. Mater.* **19** (2007) 4297-4306.
19. Y.E. Seidel, R. Lindström, Z. Jusys, J. Cai, U. Wiedwald, P. Ziemann, and R.J. Behm, *Nanostructured Pt/GC model electrodes prepared by deposition of metal-salt loaded micelles*, *Langmuir* **23** (2007) 5795-5801.
20. R.K. Ahluwalia and X. Wang, *J. Power Sources* **180** (2008) 122-131.
21. G. Stalnionis, L. Tamasauskaite-Tamasiunaite, V. Pautieniene, and Z. Jusys, *CO electrooxidation on a polycrystalline Pt electrode: A wall-jet EQCN study*, *J. Electroanal. Chem.* **590** (2006) 198-206.
22. D.J.L. Brett, P. Aguiar, N.P. Brandon, and A.R. Kucernak, *Int. J. Hydrogen Energy* **32** (2007) 863-871.
23. J. Solla-Gullon, E. Herrero, F.J. Vidal-Iglesias, J. Feliu, and A. Aldaz, *Electrochem. Comm.* **8** (2006) 189-194.
24. A. Wicowski, E. R. Savinova, and C. G. Vayenas, (Marcel Dekker, Inc., New York, 2003).
25. H. Kita, H. Narumi, S. Ye, and H. Naohara, *J. Appl. Electrochem.* **23** (1993) 589-596.
26. T.H.M. Housmans, C.G.M. Hermse, and M.T.M. Koper, *J. Electroanal. Chem.* **607** (2007) 69-82.
27. Y.E. Seidel, Z. Jusys, B. Wickman, B. Kasemo, and R.J. Behm, to be published.
28. S.G. Weber and J.T. Long, *Anal. Chem.* **60** (1988) 903A-913A.
29. A.J. Bard and L.R. Faulkner, *Electrochemical Methods*, (Wiley & Sons, New York, 1980).

30. W.E. Morf, *Anal. Chim. Acta* **341** (1997) 121-127.
31. W.E. Morf, M. Koudelka-Hep, and N.F. de Rooij, *J. Electroanal. Chem.* **590** (2006) 47-56.
32. A. Damjanovic, M.A. Genshaw, and J.O. Bockris, *J. Chem. Phys.* **45** (1966) 4067.
33. Y.E. Seidel, A. Schneider, Z. Jusys, B. Wickman, B. Kasemo, and R.J. Behm, to be published.
34. J.M. Thomas and W.J. Thomas, *Principles and Practice of Heterogeneous Catalysis*, (VCH, Weinheim, 1997).
35. V.S. Bagotzky, Y.B. Vassiliev, and O.A. Khazova, *J. Electroanal. Chem.* **81** (1977) 229-238.
36. Z. Jusys, J. Kaiser, and R.J. Behm, *Electrooxidation of CO and H₂CO mixtures on a carbon supported Pt catalyst - A kinetic and mechanistic study by Differential Electrochemical Mass Spectrometry*, *Phys. Chem. Chem. Phys.* **3** (2001) 4650-4660.
37. C. Saravanan, N.M. Markovic, M. Head-Gordon, and P.N. Ross, *J. Chem. Phys.* **114** (2001) 6404-6412.
38. B. Kasemo, S. Johansson, H. Persson, P. Thormahlen, and V.P. Zhdanov, *Topics Catal.* **13** (2000) 43-53.